Title
Open-top selective plane illumination microscope for conventionally mounted specimens

Journal
Optics Express, 23(12)

ISSN
1094-4087

Authors
McGorty, Ryan
Liu, Harrison
Kamiyama, Daichi
et al.

Publication Date
2015-06-15

DOI
10.1364/oe.23.016142

Peer reviewed

Open-top selective plane illumination microscope for conventionally mounted specimens

Ryan McGorty,[1] Harrison Liu,[2] Daichi Kamiyama,[1] Zhiqiang Dong,[3] Su Guo,[3] and Bo Huang[1,4,*]

[1]*Department of Pharmaceutical Chemistry, University of California, San Francisco, San Francisco, CA 94158, USA*
[2]*UC Berkeley - UCSF Graduate Program in Bioengineering, University of California, San Francisco, San Francisco, CA 94158, USA*
[3]*Department of Bioengineering and Therapeutic Sciences, University of California, San Francisco, San Francisco, CA 94158, USA*
[4]*Department of Biochemistry and Biophysics, University of California, San Francisco, San Francisco, CA 94158, USA*
[*]*bo.huang@ucsf.edu*

Abstract: We have developed a new open-top selective plane illumination microscope (SPIM) compatible with microfluidic devices, multi-well plates, and other sample formats used in conventional inverted microscopy. Its key element is a water prism that compensates for the aberrations introduced when imaging at 45 degrees through a coverglass. We have demonstrated its unique high-content imaging capability by recording *Drosophila* embryo development in environmentally-controlled microfluidic channels and imaging zebrafish embryos in 96-well plates. We have also shown the imaging of *C. elegans* and moving *Drosophila* larvae on coverslips.

OCIS codes: (180.2520) Fluorescence microscopy; (170.6900) Three-dimensional microscopy.

References and links

1. J. Huisken, J. Swoger, F. Del Bene, J. Wittbrodt, and E. H. K. Stelzer, "Optical sectioning deep inside live embryos by selective plane illumination microscopy," Science **305**(5686), 1007–1009 (2004).
2. H.-U. Dodt, U. Leischner, A. Schierloh, N. Jährling, C. P. Mauch, K. Deininger, J. M. Deussing, M. Eder, W. Zieglgänsberger, and K. Becker, "Ultramicroscopy: three-dimensional visualization of neuronal networks in the whole mouse brain," Nat. Methods **4**(4), 331–336 (2007).
3. J. Huisken and D. Y. Stainier, "Selective plane illumination microscopy techniques in developmental biology," Development **136**(12), 1963–1975 (2009).
4. R. Tomer, K. Khairy, and P. J. Keller, "Shedding light on the system: studying embryonic development with light sheet microscopy," Curr. Opin. Genet. Dev. **21**(5), 558–565 (2011).
5. Y. Wu, A. Ghitani, R. Christensen, A. Santella, Z. Du, G. Rondeau, Z. Bao, D. Colón-Ramos, and H. Shroff, "Inverted selective plane illumination microscopy (iSPIM) enables coupled cell identity lineaging and neurodevelopmental imaging in *Caenorhabditis elegans*," Proc. Natl. Acad. Sci. U.S.A. **108**(43), 17708–17713 (2011).
6. T. F. Holekamp, D. Turaga, and T. E. Holy, "Fast three-dimensional fluorescence imaging of activity in neural populations by objective-coupled planar illumination microscopy," Neuron **57**(5), 661–672 (2008).
7. B.-C. Chen, W. R. Legant, K. Wang, L. Shao, D. E. Milkie, M. W. Davidson, C. Janetopoulos, X. S. Wu, J. A. Hammer 3rd, Z. Liu, B. P. English, Y. Mimori-Kiyosue, D. P. Romero, A. T. Ritter, J. Lippincott-Schwartz, L. Fritz-Laylin, R. D. Mullins, D. M. Mitchell, J. N. Bembenek, A.-C. Reymann, R. Böhme, S. W. Grill, J. T. Wang, G. Seydoux, U. S. Tulu, D. P. Kiehart, and E. Betzig, "Lattice light-sheet microscopy: imaging molecules to embryos at high spatiotemporal resolution," Science **346**(6208), 1257998–1258010 (2014).
8. F. Cutrale and E. Gratton, "Inclined selective plane illumination microscopy adaptor for conventional microscopes," Microsc. Res. Tech. **75**(11), 1461–1466 (2012).
9. M. Tokunaga, N. Imamoto, and K. Sakata-Sogawa, "Highly inclined thin illumination enables clear single-molecule imaging in cells," Nat. Methods **5**(2), 159–161 (2008).
10. J. C. M. Gebhardt, D. M. Suter, R. Roy, Z. W. Zhao, A. R. Chapman, S. Basu, T. Maniatis, and X. S. Xie, "Single-molecule imaging of transcription factor binding to DNA in live mammalian cells," Nat. Methods **10**(5), 421–426 (2013).
11. M. B. Bouchard, V. Voleti, C. S. Mendes, C. Lacefield, W. B. Grueber, R. S. Mann, R. M. Bruno, and E. M. C. Hillman, "Swept confocally-aligned planar excitation (SCAPE) microscopy for high speed volumetric imaging of behaving organisms," Nat. Photonics **9**(2), 113–119 (2015).

#239835 - $15.00 USD Received 29 Apr 2015; revised 5 Jun 2015; accepted 5 Jun 2015; published 9 Jun 2015

12. Y. Wu, P. Wawrzusin, J. Senseney, R. S. Fischer, R. Christensen, A. Santella, A. G. York, P. W. Winter, C. M. Waterman, Z. Bao, D. A. Colón-Ramos, M. McAuliffe, and H. Shroff, "Spatially isotropic four-dimensional imaging with dual-view plane illumination microscopy," Nat. Biotechnol. **31**(11), 1032–1038 (2013).
13. A. Kumar, Y. Wu, R. Christensen, P. Chandris, W. Gandler, E. McCreedy, A. Bokinsky, D. A. Colón-Ramos, Z. Bao, M. McAuliffe, G. Rondeau, and H. Shroff, "Dual-view plane illumination microscopy for rapid and spatially isotropic imaging," Nat. Protoc. **9**(11), 2555–2573 (2014).
14. E. M. Lucchetta, J. H. Lee, L. A. Fu, N. H. Patel, and R. F. Ismagilov, "Dynamics of *Drosophila* embryonic patterning network perturbed in space and time using microfluidics," Nature **434**(7037), 1134–1138 (2005).
15. N. Vladimirov, Y. Mu, T. Kawashima, D. V. Bennett, C.-T. Yang, L. L. Looger, P. J. Keller, J. Freeman, and M. B. Ahrens, "Light-sheet functional imaging in fictively behaving zebrafish," Nat. Methods **11**(9), 883–884 (2014).
16. P. J. Keller, A. D. Schmidt, J. Wittbrodt, and E. H. K. Stelzer, "Reconstruction of zebrafish early embryonic development by scanned light sheet microscopy," Science **322**(5904), 1065–1069 (2008).
17. P. J. Keller, A. D. Schmidt, A. Santella, K. Khairy, Z. Bao, J. Wittbrodt, and E. H. K. Stelzer, "Fast, high-contrast imaging of animal development with scanned light sheet-based structured-illumination microscopy," Nat. Methods **7**(8), 637–642 (2010).
18. T. A. Planchon, L. Gao, D. E. Milkie, M. W. Davidson, J. A. Galbraith, C. G. Galbraith, and E. Betzig, "Rapid three-dimensional isotropic imaging of living cells using Bessel beam plane illumination," Nat. Methods **8**(5), 417–423 (2011).
19. D. Turaga and T. E. Holy, "Image-based calibration of a deformable mirror in wide-field microscopy," Appl. Opt. **49**(11), 2030–2040 (2010).
20. C. Bourgenot, C. D. Saunter, J. M. Taylor, J. M. Girkin, and G. D. Love, "3D adaptive optics in a light sheet microscope," Opt. Express **20**(12), 13252–13261 (2012).
21. P. J. Verveer, J. Swoger, F. Pampaloni, K. Greger, M. Marcello, and E. H. K. Stelzer, "High-resolution three-dimensional imaging of large specimens with light sheet-based microscopy," Nat. Methods **4**(4), 311–313 (2007).
22. M. D. Rand, J. C. Dao, and T. A. Clason, "Methylmercury disruption of embryonic neural development in *Drosophila*," Neurotoxicology **30**(5), 794–802 (2009).
23. N. L. Jeon, S. K. W. Dertinger, D. T. Chiu, I. S. Choi, A. D. Stroock, and G. M. Whitesides, "Generation of Solution and Surface Gradients Using Microfluidic Systems," Langmuir **16**(22), 8311–8316 (2000).
24. J. Schindelin, I. Arganda-Carreras, E. Frise, V. Kaynig, M. Longair, T. Pietzsch, S. Preibisch, C. Rueden, S. Saalfeld, B. Schmid, J.-Y. Tinevez, D. J. White, V. Hartenstein, K. Eliceiri, P. Tomancak, and A. Cardona, "Fiji: an open-source platform for biological-image analysis," Nat. Methods **9**(7), 676–682 (2012).

1. Introduction

Selective plane illumination microscopy (SPIM) [1,2] in recent years has demonstrated its advantages over other optical sectioning techniques in fast volumetric imaging and much reduced phototoxicity. These advantages have made SPIM an attractive technique particularly for the imaging of developing embryos and the recording of whole brain activity [2–4]. In the most common configuration of SPIM, the illumination and detection objectives are placed orthogonally on two sides of a liquid filled chamber. The illumination objective generates a light sheet that is restricted to the focal plane of the detection objective. The specimen is immobilized within a cylinder of gel placed vertically in the chamber. Volumetric imaging is achieved by scanning and/or sample rotation. An alternative configuration for SPIM is to have two water-dipping objectives oriented down at 45 degree into a petri dish [5–7], allowing the imaging of flat cell culture. Additionally, SPIM microscopes have been developed using a single high-numerical-aperture (NA) objective [8–10], but they are typically not designed for whole organism imaging except for one recently reported [11].

One important microscopy application that has not benefited from SPIM is high-content imaging which is used to systematically screen a large number of samples. For this purpose, multi-well plates or microfluidic chips are often used to enable the manipulation of the specimen and control of conditions. However, the small sized wells in multi-well plates and the planar layout of polymer microfluidic chips and the need of tubing connection makes them inconvenient to be used on existing SPIM configurations. Therefore, we sought to develop a new "open-top" configuration for SPIM that has all the imaging optics located underneath the sample. This configuration should not only allow the use of microfluidic chips and multi-well plates, but also the imaging of samples mounted in any of the common formats used with regular inverted microscopes, such as samples in small dishes or directly on top of a piece of coverglass.

#239835 - $15.00 USD Received 29 Apr 2015; revised 5 Jun 2015; accepted 5 Jun 2015; published 9 Jun 2015

2. Results

2.1 Construction of the open-top SPIM system

To develop our open-top SPIM system, we placed the illumination and detection objectives below the sample at 45 degrees to the sample stage, as shown in Fig. 1(a). This configuration resembles the *i*SPIM configuration [5,12], but differs in that both objectives sit at the opposite side of the coverglass from the sample. Such an arrangement frees the sample side of the coverglass, making it compatible with small dishes, flow cells and microfluidic chips. However, this arrangement also brings in major practical challenges: the two objectives no longer directly interface with the sample through water or air. Instead, both illumination and detection optical paths now cross a piece of coverslip at 45 degrees. With air on one side and the sample medium on the other, this arrangement produces enormous optical aberrations, rendering the microscope useless. To solve this problem, we built a water-filled prism using a 3D printed scaffold and two pieces of coverslip. This prism is held beneath the sample holder, with water in direct contact with the sample coverslip to allow free translation of the holder. Both air objectives (20 × 0.42 NA for excitation and 10 × 0.3 NA for imaging) focus perpendicularly through glass windows on the sides of this water prism. A cylindrical lens is inserted in the excitation light path for the 20 × objective to generate a light sheet with a thickness of approximately 5 μm.

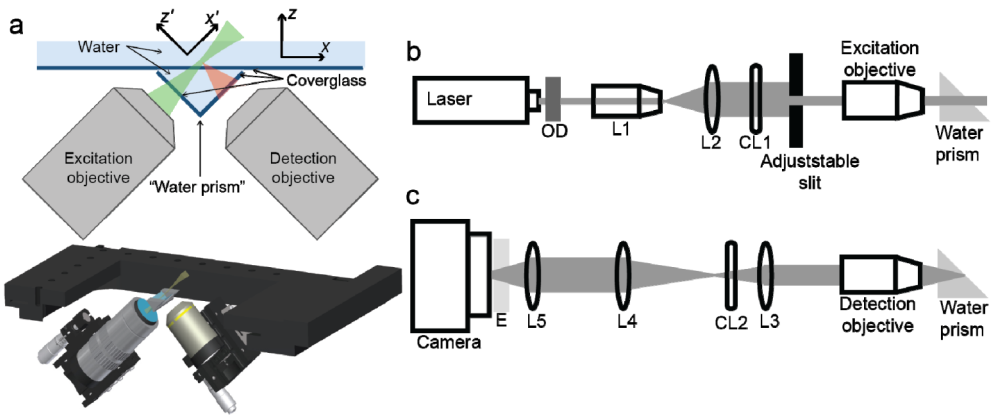

Fig. 1. Imaging with open-top SPIM (a) Schematic drawing of open-top SPIM with the two objectives beneath the sample stage. Beneath the 2D drawing we show a 3D rendering of the microscope. (b) Detailed excitation path. The laser passes through an optical density filter (OD), a 7 × beam expander consisting of a 10 × objective (L1, RMS10X, Thorlabs) and a 75 mm lens (L2, AC254-075-A, Thorlabs), a 200 mm focal length cylindrical lens (CL1, LJ1653RM-A, Thorlabs), an adjustable slit aperture, and a 20 × 0.42NA objective before going through the water prism and into the sample. (c) Emission path. The light is collected through the water prism by a 10 × 0.3NA objective, goes through the tube lens (L3, AC254-200-A, Thorlabs), the aberration-correcting cylindrical lens (CL2, SCX-50.8-5000.0, Melles Griot), a pair of lenses relaying the image to the camera (L4 and L5, AC254-075-A-ML and AC254-150-A-ML, Thorlabs), and an emission filter (E, ET525/50 or ET595/50, Chroma).

Although the water prism cancels out the aberration from imaging across a 45 degree glass-air interface, the sample coverslip still introduces astigmatic aberrations because it sits at 45 degrees with respect to the optical axis of the detection objective. This aberration is apparent in the measured point spread function (PSF) [Fig. 2(a)] as well as in Zemax ray-tracing [Fig. 2(g)]. To correct this astigmatism, we inserted a weak cylindrical lens after the tube lens of the detection objective, as shown in Figs. 2(b) and 2(h). More details of the optical layout are presented in Section *4. Materials and methods*.

A similar astigmatic aberration is expected on the illumination side, although it has much less profound consequences for the simpler task of focusing the excitation laser into a light sheet. In addition, we use an adjustable slit in the illumination path to effectively reduce the

#239835 - $15.00 USD Received 29 Apr 2015; revised 5 Jun 2015; accepted 5 Jun 2015; published 9 Jun 2015

NA of the illumination objective. Such a method to reduce the NA of the illumination objective is often done to extend the length of the light sheet along the optical axis [2,13]. In our system, it also works to inhibit the aberrations that would present themselves at higher NA.

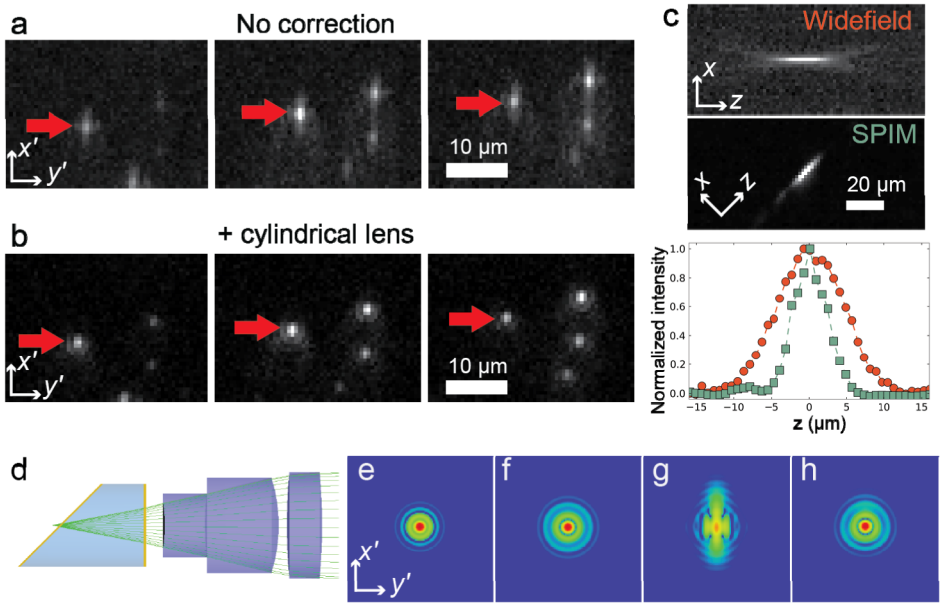

Fig. 2. Characterization of the open-SPIM. (a) Three images of 200 nm fluorescent beads embedded in agarose from a scan of the sample. Between each frame the sample has moved 2.5 μm in *x*. The shape of the PSF clearly shows astigmatism. (b) Same beads with the cylindrical lens inserted. (c) Comparison of the PSF for the same 10 × 0.3 NA objective used in a widefield microscope and in our open-top SPIM. (d) Rendering of water prism and the first three elements of an objective lens used in Zemax ray tracing software for computing the Huygen's PSFs shown in (e)-(h). The PSFs are displayed on with a log scale and cover a 330 × 330 μm^2 area under the following conditions: (e) when imaging 500 μm into water past a coverslip; (f) same as (e) with an additional 6 mm of water plus an additional coverslip between the objective and focal plane; (g) same as (f) but when the coverslip closest to the focal plane is tilted 45°; and (h) same as (g) but with a 10 m focal length cylindrical lens inserted after the tube lens.

We characterized the point spread function (PSF) of our microscope by imaging 200-nm beads embedded in 2% agarose gel across a field-of-view of approximately 300 μm × 300 μm (Fig. 2). The full-width half-maximum (FWHM) of the measured PSFs of 50 beads were 1.1 ± 0.03 μm in the lateral direction and 6.2 ± 0.6 μm in the axial direction (mean ± standard deviation), respectively. The larger axial width variation mainly reflects the increase in light sheet thickness away from focus of the illumination objective (FWHM of 5.9 μm for the 29 beads within a region of 150 μm around the tightest focus of the light sheet, versus 6.5 μm for the 21 beads outside this region). In comparison, the same 10 × imaging objective on a regular wide-field inverted microscope produces a PSF size of 0.9 μm and 10.9 μm [Fig. 2(c)]. The similar lateral widths indicate that the cylindrical lens in the imaging path has efficiently corrected the astigmatic aberrations, while the small axial width for our SPIM system is the result of optical sectioning by light-sheet illumination.

To acquire 3D data, we simply scanned the sample stage so that the specimen moves at a constant velocity through the stationary light sheet. This method of capturing volumetric data is straightforward to implement as the only required moving part is a motorized sample stage. More importantly, it allows us to cover a large volume only bounded by the travel range of the stage in *x* and *y* and by the extent of the light sheet in *z*. Stages with additional travel in *z*, (for example, a piezo *z* stage), could allow a larger sample volume to be scanned through the

#239835 - $15.00 USD Received 29 Apr 2015; revised 5 Jun 2015; accepted 5 Jun 2015; published 9 Jun 2015

light sheet. Typically, we move the stage at speeds of between 20 and 100 μm/sec and acquire images at 20 to 100 Hz when imaging stationary or slowly moving specimens, although our motorized stage and camera could achieve much higher speeds. This process is illustrated in imaging *Caenorhabditis elegans* (confined between a glass slide and coverslip) expressing GFP in PVD sensory neurons or nuclei of intestinal cells, shown in Fig. 3. The camera records slices at a 45 degree angle relative to the scanning direction. We use the coordinates *x*' and *y*' to refer to the plane recorded directly on the camera. The stack of images captured is transformed (see Appendix) to generate slices in the *x*-*y* plane [Fig. 3(a) and Media 1] and *z* projections [Fig. 3(b)], which can be used for 3D reconstruction (see Media 2).

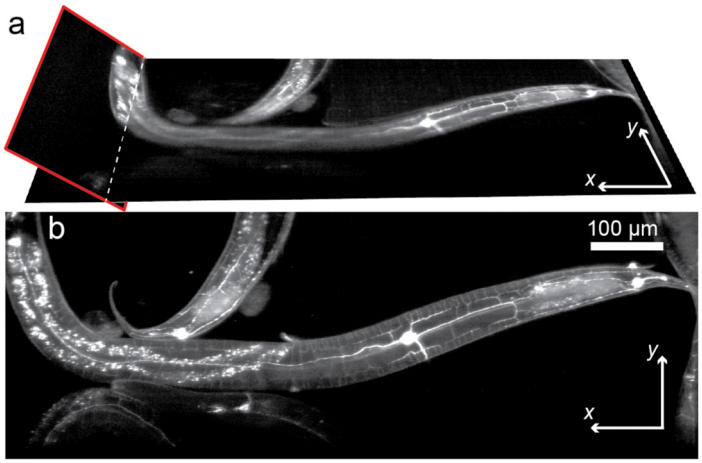

Fig. 3. (a) Two slices through volumetric data of *C. Elegans* with PVD sensory neurons labeled with GFP. The slice outlined in red shows the raw camera image prior to any transformation. The other slice is an *x*-*y* section of the transformed volumetric data. (b) *z*-projection of data shown in (a) (see Media 1 and Media 2).

2.2 Imaging Drosophila development in microfluidic channels

For the study of embryo development, the large scan range of our microscope enables simultaneous imaging of many embryos for parallel analysis. To demonstrate this capability, we imaged a large number of developing *Drosophila* embryos with GFP-expressing central nervous system (CNS) neurons in a PDMS microfluidic device containing a single, snaking channel that has multiple 14-mm long straight sections, which is depicted in Fig. 4. We designed the channel dimension so that, when loaded in, the embryos can line up single-file with their anterior-posterior axis along the channel in a given straight section. To ensure embryo viability, we used a syringe pump to flow solution through the channel. Given that an embryo is approximately 400 μm long, we were able to load 32 of them along a straight section of our microfluidic channel. Then, by scanning the stage linearly along the length of the channel, we captured optical sections of all embryos (Fig. 4 and Media 3). We managed to acquire one 3D data set of all 32 embryos in a $0.2 \times 0.22 \times 14$ mm^3 volume in as short as 2.3 minutes, with the stage scanned at a speed of 100 μm/sec and the camera recording at 100 Hz. The light exposure for each embryo was estimated to be approximately 2.4 mJ during each scan, which is comparable to reported value for other SPIM systems [5]. This low light dosage allowed us to record the development of these embryos for about 12 hours at 40 min interval and with minimum phototoxicity, as indicated by the expected morphogenesis process of their CNS.

Integration of SPIM with microfluidic devices allows the screening of embryo development under precisely controlled conditions. As a demonstration, we fabricated a more complicated device that maintained a 0 to 200 μM linear gradient of methylmercury chloride along a straight channel. Utilizing this device, we have recorded the full methylmercury

#239835 - $15.00 USD Received 29 Apr 2015; revised 5 Jun 2015; accepted 5 Jun 2015; published 9 Jun 2015

dosage-response data set on CNS development disruption in one single imaging experiment. Over 36 hours, the condensation of the ventral nerve cord which normally occurs at 13 to 16 hours after egg laying (AEL) was observed in only six embryos at the lowest end of the gradient (Fig. 5 and Media 4). Similar devices could be used for systematic characterization of *Drosophila* embryo development under other controlled conditions such as specific enzyme inhibitors and even temperature [14].

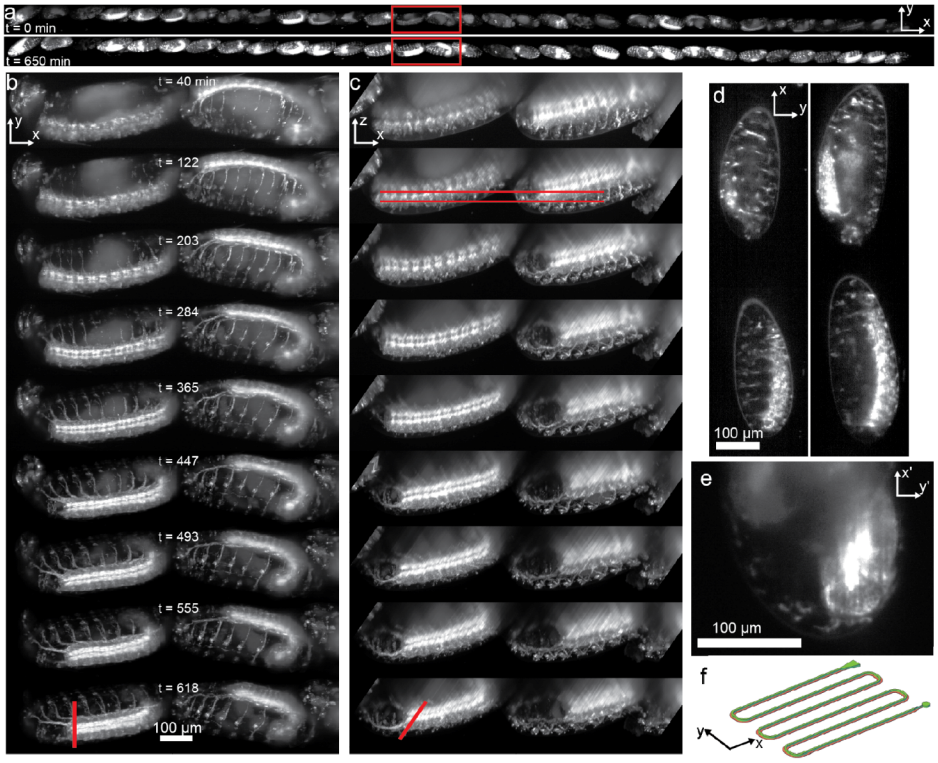

Fig. 4. Parallel imaging of developing *Drosophila* embryos. (a) The *z*-projections of 32 *Drosophila* embryos that have been loaded into an approximately 14 mm section of a microfluidic channel. Only every 10th frame was used to generate the figure. A *z*-projection is shown at t = 0 (top) and at t = 650 min. (bottom). (b) The two embryos in the red box in (a) are shown at different times. The images again display *z*-projections but all frames acquired were used. (c) The same embryos and same time points as (b) are shown as *y*-projections. (d) Two slices in the *x*-*y* plane are shown corresponding to the red lines in (c) (see Media 3). (e) Image of embryo as acquired by camera and corresponding to the position indicated by the red lines in the last time point in (b) and (c). (f) Shown is a drawing of the microfluidic channel used.

#239835 - $15.00 USD Received 29 Apr 2015; revised 5 Jun 2015; accepted 5 Jun 2015; published 9 Jun 2015

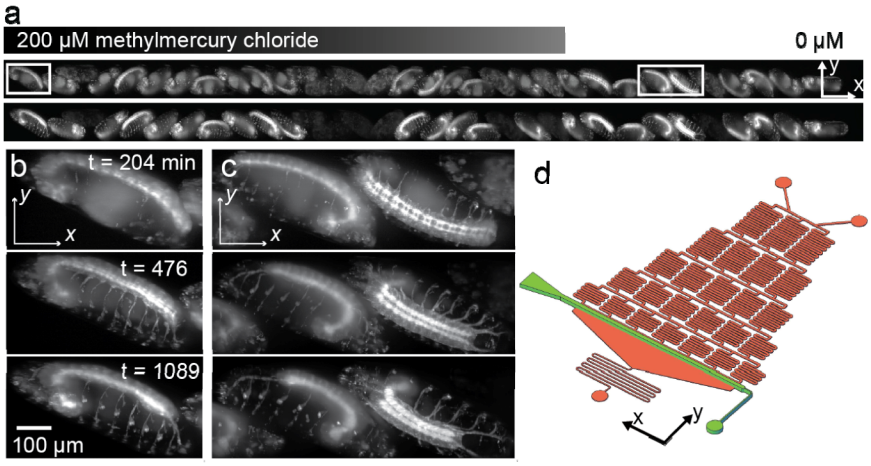

Fig. 5. Imaging of developing *Drosophila* (a) Shown are *z*-projections of 32 *Drosophila* embryos loaded into a straight microfluidic channel along which a decreasing gradient in methylmercury chloride runs from left to right at time t = 0 (top) and t = 1089 min. (bottom). Only every 6th frame recorded was used to generate the projections. (b) The embryos in the left red box in (a) at different time points. The images again display *z*-projections but all frames acquired were used. (c) The *z*-projections of the embryo in the right red box at the same times points as (b) (see Media 4). (d) The schematic drawing of the microfluidic device shows the embryo-containing channel in green and the gradient generation channels in orange.

2.3 Imaging of moving Drosophila larva

The open-top nature of our SPIM system also enables the imaging of certain freely behaving animals. We demonstrated this capability by recording first instar larvae (36:00 AEL) of *Drosophila* with CNS neurons expressing GFP moving in water atop a coverslip. To ensure that the crawling of the larvae is along the microscope scanning direction, we placed two pieces of coverslips side-by-side on top of another piece of coverslip to form a trough approximately 300 µm wide and 1.5 cm long. A glass slide was taped to the top for support. We trapped 4 larvae in a roughly 1 cm section of the trough. To reduce potential motion blur, we used a scanning speed of 800 µm/sec (120 Hz camera recording). A time sequence of SPIM images were acquired at approximately 22 sec intervals (Fig. 6) (the interval can be as short as 1.3 sec if only one larva is imaged). During recording, the larvae exhibited different speeds of movement and even inversion of moving direction. Combined with genetically encoded calcium sensors [15], our SPIM system could be potentially used to follow neuronal activity in these freely behaving larvae.

#239835 - $15.00 USD Received 29 Apr 2015; revised 5 Jun 2015; accepted 5 Jun 2015; published 9 Jun 2015

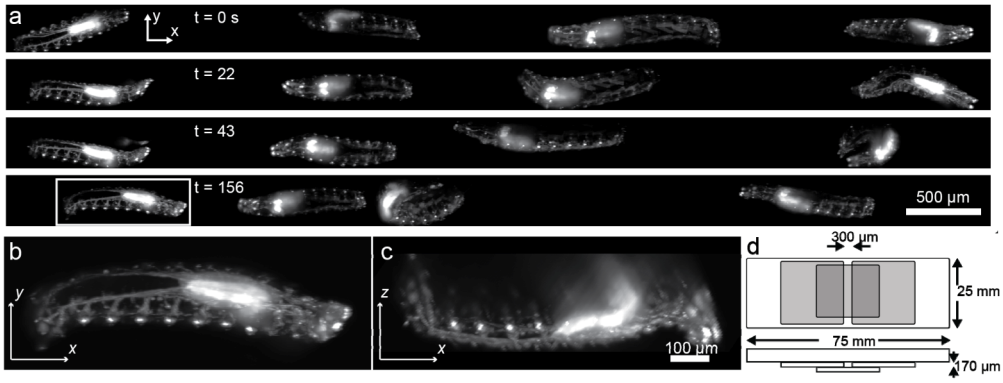

Fig. 6. Imaging crawling *Drosophila* larvae (a) *z*-projections of four moving first instar larvae at different time points. (b) A *z*-projection of the larva highlighted. (c) A *y*-projection of the same larva shown in (b). (d) Sketch of slide and coverslips used to create channel to hold moving larvae.

2.3 Fast 3D imaging in multi-well plates

Lastly, we highlight the potential of open-top SPIM to perform whole-organism phenotypic screening by imaging zebrafish embryos in a 96-well plate. We placed 48 hours post-fertilized embryos with mRFP or tdTomato tagging either the nucleus or plasma membrane, respectively, in a glass-bottomed 96-well plate and allowed them to settle to the bottom. Figure 7 displays the 3D images acquired by our SPIM system. The nuclei or the membrane of individual cells can be clearly resolved throughout the fish embryo, which could enable to detailed characterization of development defects. At a scanning speed of 20 µm/sec and camera recording rate of 20 Hz, we were able to acquire a full 3D scan in 95 sec for one embryo. On the other hand, when fixing the stage position to a single focal plane, we were additionally able to use continuous 60 Hz recording to monitor the heartbeat and blood flow in the embryo (see Media 5). In both scanning and non-scanning cases, our imaging speed is largely limited by the camera frame rate. With our capability of accumulating 3D images while scanning from one well to the next, our system could read through multiple wells in one continuous scan without stopping the stage, thus enabling fast, high-through imaging that is essential in drug or mutation screening.

#239835 - $15.00 USD Received 29 Apr 2015; revised 5 Jun 2015; accepted 5 Jun 2015; published 9 Jun 2015

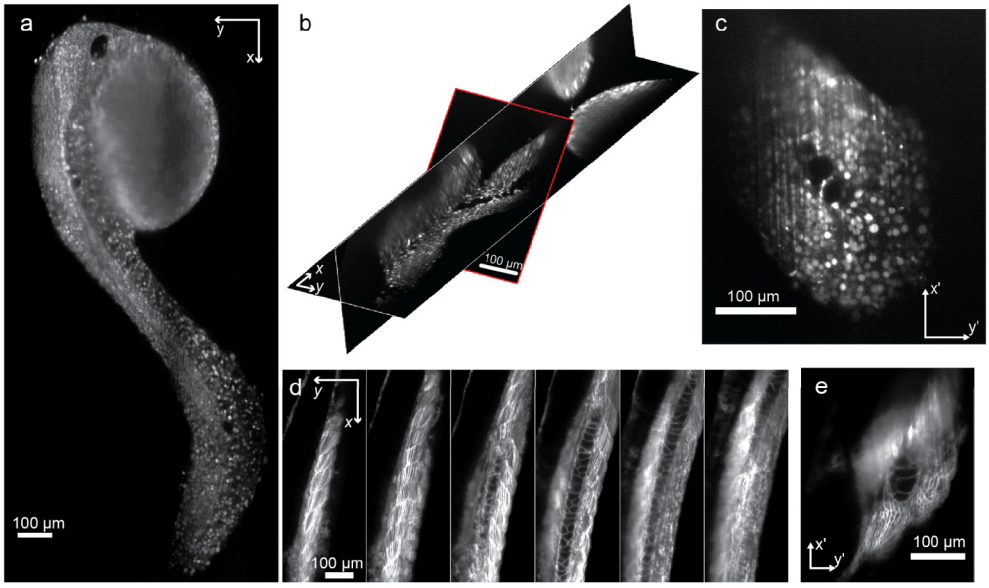

Fig. 7. Imaging zebrafish in 96-well plates (a) One *x*-*y* slice of a 48 hpf zebrafish in a 96-well plate. All cell nuclei are labeled with mRFP. (b) Multiple slices from the same embryo shown in (a). The slice outlined in red is the raw camera image before any transformations. The other two slices show an *x*-*y* and *x*-*z* cut. (c) An image of the same embryo as recorded on the camera. (d) Six *x*-*y* slices through the tail of a zebrafish with tdTomato labeling of the cell membranes. Each slice is spaced 23 µm apart in z. (e) An image as recorded by the camera of the same embryo as shown in (d) (see Media 5).

3. Discussion

Here we have demonstrated the capabilities of our open-top SPIM system to image samples prepared in formats common to high-content imaging and regular inverted microscopy methods. This allows SPIM to be paired with powerful and versatile microfluidic devices. With this pairing we obtained 3D images of many embryos developing in parallel for over a day and were able to quickly screen for the effect of methylmercury concentration on embryo development. In addition to being compatible with microfluidic devices, our open-top SPIM accepts traditionally used sample holders like multi-well plates. Our imaging of zebrafish embryos in a 96-well plate demonstrates how our microscope may be easily inserted into existing high-throughput workflows. Other sample holders may be used as well, provided the bottom surface is made of glass coverslip, which allowed us to image whole crawling *Drosophila* larvae.

In designing an open-top SPIM, we have focused our efforts on making it straightforward to implement and usable with an assortment of commonly used sample formats. Therefore, the reported system has not been specifically optimized for image quality or spatial resolution. Indeed, many previous methods to reduce sample shadowing, enhance illumination homogeneity and improve 3D resolution could be adapted to our platform, including the generation of the light sheet by scanning a focused laser beam [16,17], the use of Bessel beam illumination [18], and the dual-view SPIM configuration which alternatively illuminates and detects fluorescence from both objectives [12]. What would not be compatible with our configuration is multi-view imaging by rotating the sample [1] which would improve the imaging homogeneity for thick samples.

On the other hand, our configuration does contain additional sources of aberration that are not present in other SPIM configurations, primarily due to imaging across the water in our prism and then a tilted coverslip. We have shown that placement of a cylindrical lens in the imaging path effectively corrects the lower-order astigmatic aberrations. Nevertheless,

#239835 - $15.00 USD Received 29 Apr 2015; revised 5 Jun 2015; accepted 5 Jun 2015; published 9 Jun 2015

higher-order aberrations, which would be especially important when using higher-NA imaging objectives, would likely require a stationary phase plate or adaptive optics [19,20]. Alternatively, corrections could be made post-acquisition with deconvolution software [21].

Finally, the imaging throughput of our SPIM system will benefit from sample holders that can organize the specimens in a linear manner. Our *Drosophila* embryo imaging in microfluidic channels perfectly illustrates this application. For 96-well plates where the well width exceeds the size of the microscope view field, specifically designed wells that confine embryos to the center of the well can allow them to be imaged in one single scan, thus improving the acquisition efficiency. Combining these sample handling methods and our open-top SPIM system, we expect to see new kinds of live imaging experiments and high-throughput screenings.

4. Materials and methods

4.1 SPIM setup

Our microscope uses 473 nm and 532 nm diode-pumped solid state lasers (MBL-FN-473-50mW and MGL-FN-532-500mW, Changchun New Industries Optoelectronics, China) for excitation. The laser light is directed through a 200 mm cylindrical lens (LJ1653RM-A, Thorlabs) and then a 20 × 0.42NA objective with a working distance of 20 mm (Mitutoyo). This illumination objective focuses the excitation light to a sheet approximately 7 mm past the window of and into the water prism. We use a 10 × 0.3NA air objective with a working distance of 15.2 mm (Nikon) for detection. The image is then directed to and captured on an sCMOS camera (Flash 4.0, Hamamatsu). A cylindrical lens of focal length 10 m (SCX-50.8-5000.0, Melles Griot) is placed after the tube lens of the detection objective for aberration correction. The placement of this cylindrical lens was determined by visually inspecting the PSF of fluorescent beads as the cylindrical lens was translated between the tube lens and the following relay lens. After the cylindrical lens, a 75 mm focal length lens followed by a 150 mm lens (AC254-075-A-ML and AC254-150-A-ML, Thorlabs) together relay the image to the camera and provides an additional 2 × magnification. Before the camera we place an emission filter (ET525/50 or ET595/50, Chroma) to block reflected laser light. A simplified schematic of the optical elements without fold mirrors is shown in Fig. 1.

Both objectives are mounted in translation stages that allow for 1/2” travel along their axes (CT1, Thorlabs). This allows us to finely align both objectives so that their focal planes overlap.

To the stationary mechanical components that hold the illumination objective we fix the water prism so that it is positioned between both objectives and directly underneath the sample stage. The water prism is constructed out of 3D printed ABS plastic (Dimension μPrint). Two 9 × 18 mm^2 pieces of coverslip glass are glued to the sides of the prism facing the two objectives. The top surface of the prism has dimensions of 18 mm × 13 mm and is left open to be filled with water. Once filled, the top surface of water contacts the glass- or plastic-coverslip bottomed sample holder, such as a multi-well plate or microfluidic device. The sample holder moves in *x* and *y* by a motorized stage (MS-2000, ASI). The stage is raised approximately 38 cm above our optical table with posts to accommodate the optical components underneath.

The power of the excitation light exiting the objective was about 120 to 480 μW when imaging the developing *Drosophila* embryos. Since it took between 5 and 20 seconds to image an entire embryo, the energy delivered to an embryo in one scan was approximately 2.4 mJ. Since a typical embryo is approximately 400 μm × 150 μm × 150 μm, the energy density was approximately 0.3 nJ/μm^3. When imaging the moving *Drosophila* larvae we used a slightly higher laser power but reduced the time to image one specimen to just over 1 second. Therefore, the energy delivered to a larva was approximately 1.1 mJ. For zebrafish imaging shown in Fig. 6, approximately 93.6 mJ was delivered to the embryo in each imaging pass.

#239835 - $15.00 USD Received 29 Apr 2015; revised 5 Jun 2015; accepted 5 Jun 2015; published 9 Jun 2015

4.2 Microfluidic device fabrication

Microfluidic devices were fabricated using standard PDMS-based soft lithography techniques. Two layered master molds were made by spin coating negative photoresist (SU-8, Microchem) 30 μm and 200 μm thick, respectively. Devices were cast using a 10:1 PDMS pre-polymer to cross-linker mix (Sylgard 184, Dow Corning). The device was de-molded and through-holes created using 1.5 mm and 0.75 mm diameter biopsy punches for embryo loading and liquid loading channels respectively (Miltex). The devices were then oxygen plasma treated (Harrick Plasma) and bonded to a glass coverslip (24 × 30 mm No. 1.5, VWR). Embryos were loaded by inserting a glass Pasteur pipette (VWR) into the device and filling the pipette with embryos suspended in PBS and 0.1% Triton X-100 (Sigma-Aldrich).

4.3 Drosophila imaging

Drosophila embryos were loaded by pipette into the microfluidic device depicted in Fig. 3(g). Such a device could hold hundreds of embryos but we loaded less than 50 embryos and only imaged those that occupied one of the straight 14 mm long sections of the channel. The channel's width and height were 215 μm and 200 μm so that embryos lined up single-file along the channel. We could not control for the embryos' dorsoventral orientation resulting in poorer quality images of the ventral nerve cord due to tissue scattering in some embryos with unfavorable orientations.

With our motorized stage we moved the sample through the light sheet in the *x*-direction to image 32 embryos. We began imaging the developing embryos by moving the stage at 20 μm/sec and recording images at 20 Hz and later increased to 100 μm/sec and 100 Hz to reduce image blur caused by twitching of the embryos. Therefore, it took either 11.5 or 2.3 minutes to image the entire row of embryos. Such scans were automatically repeated every 40 minutes for about 12 hours.

Because of the long imaging duration, water in the water-prism would evaporate. Therefore, we used a syringe pump to replenish the water at a flow rate of between 600 and 1000 μL/hour.

To observe the development of *Drosophila* exposed to a chemical gradient we used the microfluidic device depicted in Fig. 5e with methylmercury chloride, a known teratogen [22]. This device contains a single, straight channel to hold the embryos. A linear concentration gradient runs perpendicular to this channel. This method of creating a chemical gradient was adapted from literature [23]. In short, a solution of 100% PBS buffer and a solution of 200 μM methylmercury chloride in PBS were flowed into two input valves with syringe pumps and subsequent branches in the device mix and distribute the two solutions. The entire channel containing 32 embryos was automatically imaged about every 20 minutes for over 36 hours. During imaging, the stage was moved at 80 μm/sec and the camera acquired frames at 80 Hz.

We imaged living *Drosophila* larvae after placing them in a roughly 300 μm channel between a glass slide and coverslip. The edges of two coverslips acted as the walls of the channel and as spacers between the glass slide and coverslip. While moving the stage at 800 μm/sec back and forth along the length of the channel we acquired images at 120 Hz.

4.4 Image processing

In order to display images of our samples in the *x*-*y* or *x*-*z* planes as the axes in Fig. 1 indicate we need to transform the data acquired by our camera. The images acquired by our camera were loaded as stacks into Fiji [24]. We then used an affine transform comprising of a shear, scaling and rotation in order to produce an image stack aligned to the *xyz* axes.

The required amount of shear and scaling depends on the ratio of the pixel size on the camera and the distance the sample was translated by the motorized stage in *x* between adjacent frames. The size of a pixel in the sample plane corresponds to about 285 nm. We typically used 2 × 2 binning so that the new pixel size is 570 nm. If the sample was moved at 100 μm/sec and we image at 100 Hz, then the sample moved along the *x*-direction 1 μm

#239835 - $15.00 USD Received 29 Apr 2015; revised 5 Jun 2015; accepted 5 Jun 2015; published 9 Jun 2015

between consecutive frames. Therefore, we would need to shear the data by 0.57 μm / √2 / 1 μm ≈0.4. The square root of 2 enters the expression since images are recorded in a plane tilted 45° from the *x*-axis.

4.5 C. elegans sample

Strains of *C. elegans* were cultured and maintained using standard protocols. We used the strain *wdIs51* ($P_{F49H12.4}$GFP) (Fig. 3 and Media 1) which had GFP-labeled PVD sensory neurons, and the *ruIs32* ($P_{pie\text{-}1}$GFP::H2B) strain which had GFP-labeled nuclei in the intestinal cells (Media 2).

4.6 Drosophila sample

We used *Drosophila* expressing membrane-targeted GFP in all neurons (*elav-gal4(iii)/UAS-CD4::tdGFP*). Embryos were collected using standard protocols and aged for given hours on grape agar plates at 25°C. They were dechorionated in a solution of 50% bleach before imaging experiments.

4.7 Zebrafish sample

Zebrafish were maintained at UCSF in accordance with National Institutes of Health and UCSF guidelines. Individual embryos were dechorionated and placed in the wells of a 96-well plate containing Danieau's solution (NaCl 17.4 mM, KCl 0.21 mM, MgSO4·7H2O 0.12 mM, $Ca(NO3)_2$ 0.18 mM, HEPES 1.5 mM). They were cultured at 28°C. The following transgenic lines were established and used in this study: *tg[EF1α-H2BmRFP]* (in which the nuclei are fluorescently labeled) and *tg[EF1α-myrTdTomato]* (in which the cell membranes are fluorescently labeled). H2BmRFP or myrTdtomato were cloned into the transposon vector PT2KXIG, driven by the ubiquitous promoter EF1*α*, to obtain the DNA plasmids *EF1α-H2BmRFP-PT2KXIG* and *EF1α-myrTdTomato-PT2KXIG*. These DNA constructs were micro-injected together with tol2 transposase RNA into 1-cell stage wild type (AB) zebrafish embryos. We used a 532 nm laser for the mRFP and tdTomato imaging.

Appendix

A.1 Media captions

Media 1: A scan along the *z*-axis of the *C. elegans* shown in Fig. 3 with the PVD sensory neurons labeled with GFP. Each frame is separated by 1.1 μm.

Media 2: Shown is a 3D projection of a *C. elegans* with GFP-labeled nuclei in the intestinal cells.

Media 3: A scan along the *z*-axis of two developing *Drosophila* embryos shown in Fig. 4 at the time point 406 minutes. Each frame is separated by 570 nm in *z*. Following the *z*-scan is a 3D projection of the two embryos.

Media 4: Projections along the *z*-axis (top) and *y*-axis (bottom) of the two embryos developing in the chemical gradient shown in Fig. 5(c).

Media 5: Recorded movie of the heartbeat of a 48 hpf embryo in a 96-well plate. The cell membranes of the embryo have been labeled with tdTomato. The movie was recorded at 60 frames per second with the light sheet stationary and the movie is played back at 30 frames per second.

Acknowledgments

This work is supported by NIH (R21NS082938 for RM, ZD, BH and SG, R21MH101688 for DK and BH, and R01DA035680 for ZD and SG)). HL receives the NSF Graduate Fellowship. We thank Baohui Chen for helping with *C. elegans* culture. The *C. elegans* strains were provided, through Noelle L'Etoile, by the Caenorhabditis Genetics Center (NIH P40OD010440). We thank the Bloomington Drosophila stock center for fly stocks.